Front. Earth Sci. 2021, 15(2): 283–300
https://doi.org/10.1007/s11707-021-0879-8

RESEARCH ARTICLE

The influences of composition and pore structure on the adsorption behavior of CH_4 and CO_2 on shale

Xiangzeng WANG[1], Junping ZHOU (✉)[2,3], Xiao SUN (✉)[1], Shifeng TIAN[2,3], Jiren TANG[2,3], Feng SHEN[1], Jinqiao WU[1]

1 Research Institute of Yanchang Petroleum (Group) Co. Ltd, Xi'an 710052, China
2 State Key Laboratory of Coal Mine Disaster Dynamics and Control, Chongqing University, Chongqing 400044, China
3 School of Resources and Safety Engineering, Chongqing University, Chongqing 400044, China

Abstract CO_2 enhanced shale gas recovery (CO_2-ESGR) has attracted extensive attention as it can improve the shale gas recovery efficiency and sequestrate CO_2 simultaneously. In this study, the relationship between mineral composition, pore structure, CH_4 and CO_2 adsorption behavior as well as selective adsorption coefficient of CO_2 over CH_4 (α_{CO_2/CH_4}) in marine and continental shales at different temperatures was investigated. The results illustrated that shale with higher total organic carbon (TOC), higher clay minerals and lower brittle mineral contents has a larger micropores and mesopores volume and specific surface area. TOC content was positively correlated with fractal dimension D_f. Both CH_4 and CO_2 adsorption capacity in shale have positive correlations with TOC and clay mineral content. CO_2 adsorption capacity of the all the tested shale samples were greater than CH_4, and the α_{CO_2/CH_4} of shale were larger than 1.00, which indicated that using CO_2-ESGR technology to improve the gas recovery is feasible in these shale gas reservoirs. A higher TOC content and in shale corresponding to a lower α_{CO_2/CH_4} due to the organic matters show stronger affinity on CH_4 than that on CO_2. Shale with a higher brittle mineral content corresponding to a higher α_{CO_2/CH_4}, and no obvious correlation between α_{CO_2/CH_4} and clay mineral content in shale was observed due to the complexity of the clay minerals. The α_{CO_2/CH_4} of shale were decreased with increasing temperature for most cases, which indicated that a lower temperature is more favorable for the application of CO_2-ESGR technique.

Keywords shale gas, carbon dioxide sequestration, pore structure, selective adsorption, fractal dimensions

Received November 16, 2020; accepted January 24, 2021

E-mails: zhoujp1982@sina.com (Junping ZHOU),
yanchangsunxiao@163.com (Xiao SUN)

1 Introduction

Shale gas, as a kind of unconventional natural gas, has attracted worldwide attention in recent years as a clean energy with huge reserves (Dayal, 2017; Shan et al., 2017; Cui et al., 2019; Jiao, 2019; Shcherba et al., 2019; Wang et al., 2019a; Zeng et al., 2019; Kuang et al., 2020; Pang et al., 2020; Zhang et al., 2020). The CO_2 enhanced shale gas recovery (CO_2-ESGR) is a promising technology as it can promote the shale gas recovery and simultaneously sequestrate CO_2 in shale gas reservoir (Li and Elsworth., 2015; Pei et al., 2016; Zhou et al., 2019a; Iddphonce et al., 2020). Generally, shale gas is stored in reservoirs in three states, including free gas, dissolved gas and adsorbed gas. Adsorbed gases account for 20%–85% of total gas in shale gas reservoirs (Charoensuppanimit et al., 2016; Wang et al., 2016). The mechanism of CO_2-ESGR in shale is the displacement of originally adsorbed CH_4 by the injected CO_2 due to the different adsorption potential in shale between CO_2 and CH_4 (Du et al., 2019; Klewiah et al., 2020; Zhou et al., 2020). Thus, understanding the adsorption behaviors of CH_4 and CO_2 on shale is essential to determining shale gas recovery efficiency and the geological CO_2 storage potential in shale.

The adsorption behavior of CH_4 and CO_2 in shale is mainly influenced by the factors of reservoir conditions and shale properties. Reservoir conditions include temperature, pressure, *in-situ* stress and water saturation, while shale properties include total organic carbon content, maturity, mineral type and content, and pore structures (Zhou et al., 2019b; Klewiah et al., 2020; Qin et al., 2020; Zhang et al., 2020). The adsorption capacity of CH_4 and CO_2 usually show positive correlations with organic matter content and pore specific surface area in shale, while the adsorption capacity of CH_4 and CO_2 show complex relationship with brittle minerals and clay minerals,

depending on the specific mineral composition and content (Gasparik et al., 2014; Hellar and Zoback, 2014; Gu et al., 2017; Zhou et al., 2018; Zhou et al., 2019c; Klewiah et al., 2020). Generally, the adsorption capacity of CO_2 on shale is always larger than that of CH_4, however, the selective adsorption coefficient of CO_2 over CH_4 (α_{CO_2/CH_4}), which can be used as an important index to evaluate the competitive adsorption of CO_2 and CH_4, has shown a wide variation range in different shales (Duan et al., 2016; Zhou et al., 2017; Qi et al., 2018; Liu et al., 2019). The α_{CO_2/CH_4} in shale is also relevant to the pore structure, organic matter type and mineral composition of shale (Gu et al., 2017; Liu and Hou, 2020).

The nanopore/micropore inner surfaces of organic and inorganic components in shale is the main adsorption site for CH_4 and CO_2, thus, the pore structure of shale has significant influence on the adsorption behaviors of shale. Shale pore structure has strong heterogeneity, and is also related to the mineral composition of shale as shale with higher TOC, higher quartz content and lower clay content tend to contain more heterogeneous micropores (Hou et al., 2018; Zhou et al., 2018; Li et al., 2020b). Fractal theory can be used as an efficient method to quantitatively characterize the pore structure (Zhang et al., 2016; Hou et al., 2018; Li et al., 2018; Zhou et al., 2018; Feng et al., 2019; Liu et al., 2020). Theoretically, fractal dimension is an effective parameter to reflect the complexity of pore structure (Zhou et al., 2018), thus it may be a useful index to describe the adsorption behavior of shale and establish the relationship between pore structure and adsorption capacity of CH_4 and CO_2 in shale.

As multiple factors such as mineral compositions and pore structure show different influences on the adsorption capacity and selective adsorption of CH_4 and CO_2 for different shales, so it is requisite to conduct specific research on the basis of specific cases. In addition, the mineral composition, pore structure and adsorption behaviors of shale are interrelated and influence each other. In this study, the relationship between shale mineral compositions, pore structure (including the amount of micropore/mesopore/macropore, fractal characteristics) and shale adsorption characteristics of CH_4 and CO_2 (including adsorption capacity and selective adsorption coefficient) for marine shale and continental shale in different regions was determined, aims to reveal the influence of shale properties on the CH_4 and CO_2 adsorption behaviors, then further provide the guidance for the evaluation of adaptability for the application of CO_2-ESGR technology in different shale gas reservoirs.

2 Materials and methods

2.1 Samples preparation

Six shale samples were used in this study, four marine shale samples were collected from the Silurian Longmaxi Formation (three samples, labeled as LMX1, LMX2 and LMX3) and the Ordovician Wufeng Formation (one sample, labeled as WF), two continental shale samples were collected from and the Triassic Yanchang Formation (two samples, labeled as YC1 and YC2). The WF sample was obtained from outcrop, and the LMX1, LMX2, LMX3, YC1 and YC2 samples were obtained from drilling cores at the depth of 660.0 m, 679.3 m, 629.8 m, 506.9 m and 660.1 m, respectively. The mineral composition, element content and pore structure of all the collected samples were characterized by X-ray fluorescence (XRF) spectrometry, X-ray diffraction (XRD) and low-temperature nitrogen adsorption, respectively, then the relationship between mineral compositions and pore structure was determined. Four samples (two marine shale samples LM1 and WF, and two continental shale samples YC1 and YC2) were selected for CH_4 and CO_2 adsorption measurements. As shown in Fig. 1, all shale samples were powdered and sieved according to the requirements of each test object.

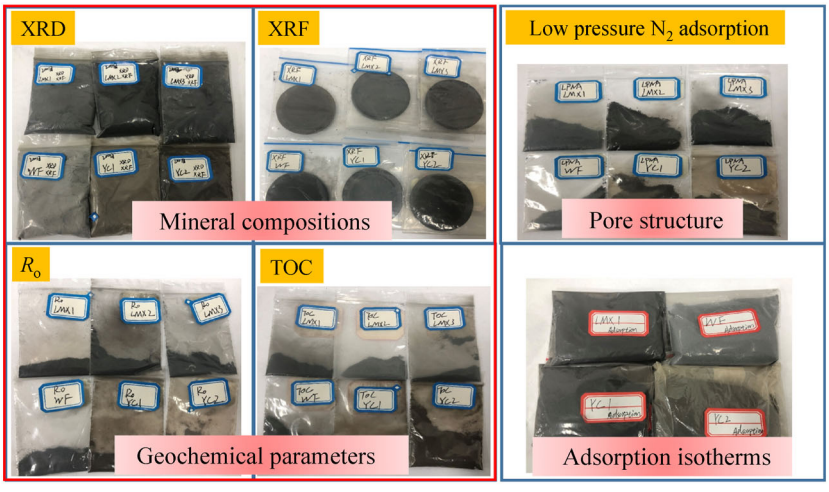

Fig. 1 Shale samples for different tests.

Samples were stored and transported in sealed bags filled with helium gas, which prevents the sample from interacting with gases in the air. The gases used in the adsorption experiments were pure CH_4 and CO_2.

2.2 Experimental section

2.2.1 Mineral compositions and geochemical parameters analysis

The element content and mineral compositions of the shale samples were determined by XRF and XRD, respectively. The XRF (RIGAKU ZSX Primus III plus) was conducted at 50 kV and 40 mA and the XRD (Rigaku D/Max-2500/PC) operated with Cu Kα radiation at 40 kV, 40 mA. Total Organic Carbon (TOC) content was obtained by Multi N/C 3100 TOC-TN analyzer (Analytik Jena, Germany). The organic maturity (R_o) was determined by Polarizing Microscope (DM 4500P, Leica, Germany).

2.2.2 Pore Structure characterization

Pore structure of shale samples was analyzed by the low pressure nitrogen (N_2) adsorption measurements. The Micrometritics ASAP 2020 system was used to obtain low pressure nitrogen (N_2) adsorption/desorption isotherms. Based on low pressure nitrogen (N_2) adsorption/desorption isotherms and IUPAC pore size classification standard ((micropores (0–2 nm), mesopores (2–50 nm), and macropores (>50 nm)) (Sing, 1982), total specific surface area (SSA_{total}), micropore (SSA_{mic}), mesopore (SSA_{mes}) and macropore (SSA_{mac})) specific surface area were calculated by Brunauer-Emmett-Teller (BET) model, and the total pore volume (PV_{total}), micropore (PV_{mic}), mesopore (PV_{mes}) and macropore (PV_{mac})) pore volume and average pore diameter (PD_{avg}) were determined by Barret-Joyner-Halenda (BJH) model (Brunauer et al., 1938; Thommes et al., 2015).

2.2.3 CH_4 and CO_2 adsorption isotherms measurements

The adsorption isotherms of CH_4 and CO_2 of shale samples were determined by the volumetric method. All the adsorption measurements were accomplished in the PCTPro Full-automatic high-pressure gas adsorption/desorption instrument of Setaram (France) (Keshavarz et al., 2017), the physical picture of the system is shown in Fig. 2. The adsorption isotherm measurements were performed at different temperatures (298.15 K, 318.15 K, and 338.15 K). To avoid the influence of residual moisture in shale on the adsorption isotherm test, all samples were dried at 105°C for 24 hours before the experiment.

3 Results and discussion

3.1 Mineral compositions and pore structure of shale samples

3.1.1 Mineral compositions

Table 1 shows the main element content of the tested shale

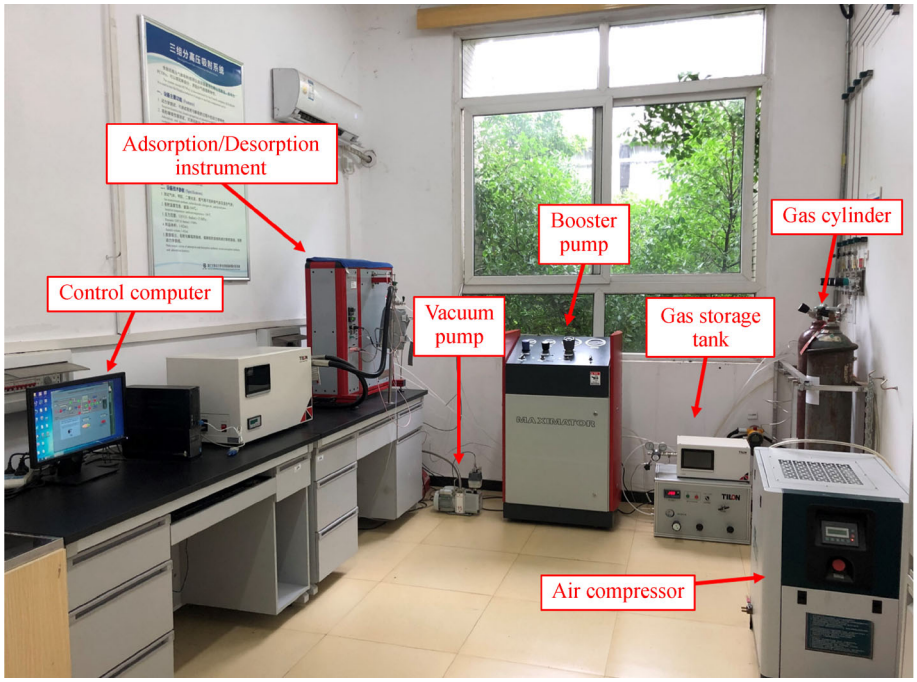

Fig. 2 PCTPro Full-automatic gas adsorption/desorption instrument of Setaram.

samples, it can be concluded that the shale samples mainly composed of elements of Si, Al, Ca, Fe, K, Mg, S, etc. In addition, a small amount of elements such as Na, Ti, Ba, P, etc., with the contents less than 1.0% wt are also contained. Table 2 shows vitrinite reflectance (R_o), the total organic carbon (TOC) content and mineral compositions of the shale samples. The range of R_o in all the tested shale samples is between 0.93%–2.76%, and the range of TOC is 1.89%–3.53%. It was found that the average values of R_o and TOC in marine shales (2.98% and 2.28%, respectively) are larger than those in continental shales (2.14% and 0.99%, respectively), which is consistent with the results of others (Yang et al., 2017; Wang and Guo, 2020). The quartz, carbonate, feldspar and clay minerals were the main mineral components of the tested shale samples. Brittle mineral contents of quartz, carbonate and feldspar for the tested shale samples were 36.6%–40.8%, 0.4%–9.2%, 4.8%–20.3%, respectively. The total content of brittle minerals is 43.9%–57.3%, which shows good fracturability (Zou et al., 2010). Clay minerals, including kaolinite, montmorillonite, illite, and chlorite, which contribute micropore volume and provide adsorption sites for gas (Lu et al., 1995; Slatt and O'Brien, 2011), accounted for a high proportion of 40.1%–54.9%.

3.1.2 Pore structure characterization

The low pressure N_2 adsorption isotherms of all the tested shale samples are shown in Fig. 3, it can be seen from that there is a significant hysteresis loop between the adsorption-desorption isotherms. The shape of hysteresis loop can reflect the micromorphology of shale pore structure. According to the IUPAC classification of hysteresis loops, the N_2 adsorption-desorption isotherms of marine shale samples belong to H2 and H3 types as the adsorption and desorption curves almost coincide in the low relative pressure area, which indicated the presence of slit-like and ink-bottle-shaped pores in shale. The N_2 adsorption-desorption isotherms of continental shale samples belong to H3 and H4 types, which are associated with slit-shaped pores and narrow slit-shaped pores (Thommes et al., 2015; Zhang et al., 2016).

Pore structure parameters determined from low pressure N_2 adsorption isotherms are listed in Table 3. The total pore volume PV_{total} ranges from 9.70–15.70$\times10^{-3}$ cm^3/g, in which PV_{mes} is dominant which ranges from 5.61–10.79$\times10^{-3}$ cm^3/g), accounting for 70.51%–89.23% of PV_{total}. The total specific surface area SSA_{total} ranges from 1.64–16.67 m^2/g, and SSA_{mes} is still dominant which

Table 1 Main element content (%) of shale samples

Wt%	LMX1	LMX2	LMX3	YC1	YC2	WF
SiO_2	66.9401	64.9386	65.5527	62.3361	63.1161	57.1634
Al_2O_3	14.5691	16.4661	18.5704	20.5182	19.6781	11.2706
Fe_2O_3	4.8543	5.5406	5.4699	6.7368	6.9415	5.9261
K_2O	3.6754	4.2640	4.8515	3.2303	3.0904	1.0944
MgO	2.4342	2.8376	2.9271	2.5447	2.4696	4.9130
SO_3	2.0545	2.2038	0.6705	0.4830	0.5164	0.7374
CaO	3.4858	1.8420	0.3081	1.3372	1.2221	18.1471
Na_2O	0.7673	0.6682	0.6473	0.9119	1.0386	0.1080
TiO_2	0.6366	0.6745	0.6273	1.1476	1.0697	0.1799
BaO	0.1044	0.1297	0.1065	0.0523	0.0474	—
P_2O_5	0.1545	0.1139	0.1054	0.3781	0.4487	0.0949

Table 2 R_o (%), TOC (%) and mineral composition content (%) of shale samples

Sample No.	R_o	TOC	Quartz	Carbonate	Feldspar	Pyrite	Clay			
							illite	kaolinite	chlorite	montmorillonite
LMX1	1.75	3.04	39.2	1.8	6.6	2.8	24.8	3.3	17.2	4.3
LMX2	2.15	3.53	37.4	0.9	5.6	1.2	32.1	1.3	18.2	3.3
LMX3	2.45	2.47	40.8	3.8	7.9	1.8	26.1	4.3	12.4	2.9
WF1	2.76	2.89	38.2	9.2	4.8	7.7	21.8	4.7	11.8	1.8
YC1	0.93	2.38	36.6	0.4	20.3	0.9	16.6	10.3	13.3	1.6
YC2	1.06	1.89	37.1	0.7	19.0	0.7	9.4	11.9	20.1	1.1

Notes: carbonate minerals are the total amount of calcite and dolomite; feldspar are the total amount of potassium feldspar and plagioclase.

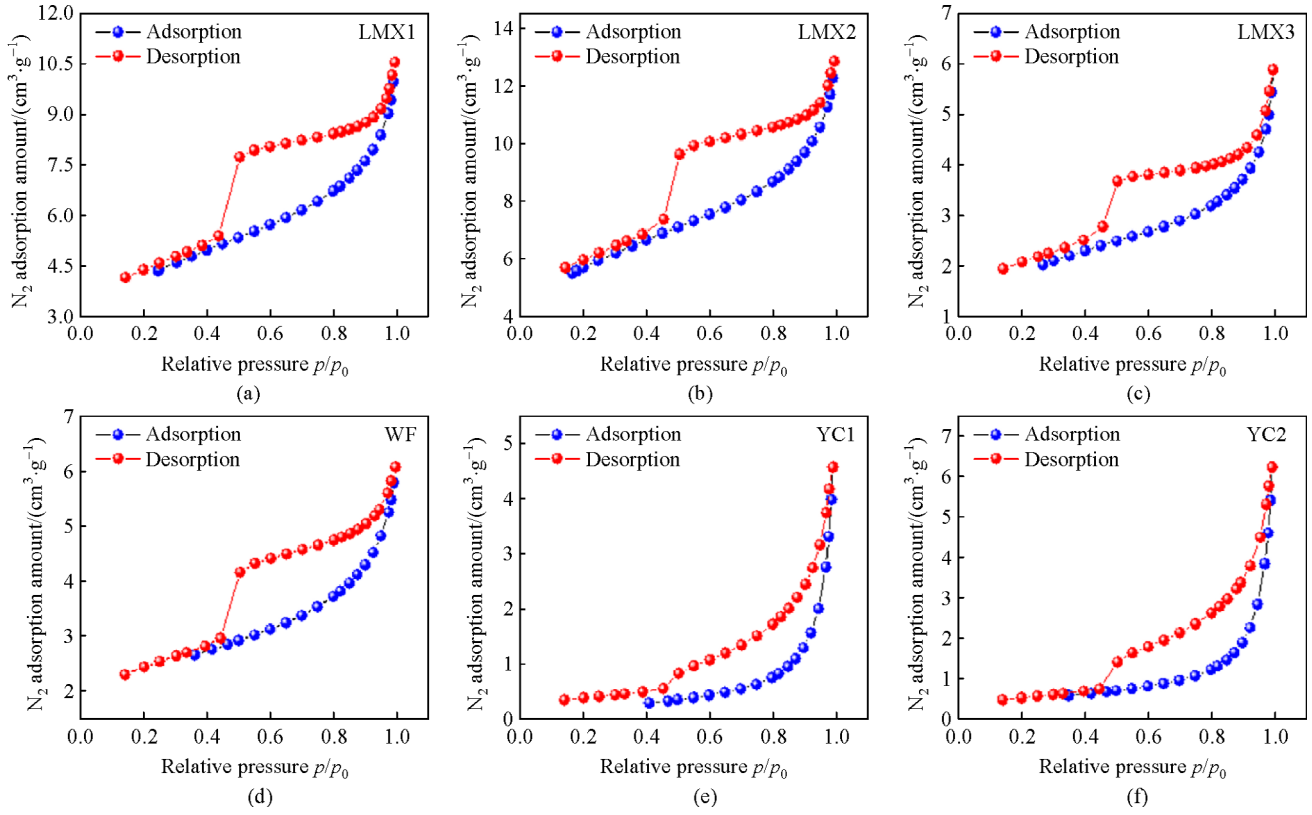

Fig. 3 N_2 adsorption-desorption isotherms of shale samples.

Table 3 Pore structure parameters of shale samples

Sample No.	Pore volume/(10^{-3} cm^3/g)				D_{ave}/nm	BET surface area/($m^2 \cdot g^{-1}$)			
	PV_{total}	PV_{mic}	PV_{mes}	PV_{mac}		SSA_{total}	SSA_{mic}	SSA_{mes}	SSA_{mac}
LMX1	15.2	2.21	10.70	2.32	4.34	12.88	3.165	9.598	0.114
LMX2	15.7	2.46	10.79	2.42	4.00	16.67	3.933	12.604	0.134
LMX3	8.8	0.93	6.50	1.36	4.82	6.03	1.434	4.540	0.053
WF	8.8	1.96	6.00	0.79	5.09	5.60	1.620	3.948	0.031
YC1	7.1	0.12	5.61	1.38	19.97	2.60	0.132	2.316	0.148
YC2	9.7	0.07	6.70	2.91	16.64	1.64	0.076	1.395	0.168

accounting for more than 68.48% of the SSA_{total}. It is worth noting that the micropore and mesopore volume of shale samples account for 69.95%–90.93% of the total pore volume, while the specific surface area of micropore and mesopore accounts for 89.74%–99.45% of the SSA_{total}, indicating that micropores and mesopores contribute the majority specific surface area in shale, and provide the majority adsorption site for gas in shale.

The irregularity of pore surface morphology and structure in porous media can be characterized by fractal theory (Li et al., 2016; Li et al., 2019). The Frenkel–Halsey–Hill (FHH) model is widely used for calculating the fractal parameters of irregular pores in heterogeneous solids based on the data of N_2 adsorption (Pomonis and Tsaousi, 2009; Cai et al., 2013).

Using the FHH model, the fractal dimension (D_f) can be determined by:

$$\ln V = A\ln[\ln(p_0/p)] + \text{constant}, \quad (1)$$

$$D_f = A + 3, \quad (2)$$

where V denotes the volume of adsorbed gas molecules at the equilibrium pressure p (MPa), cm^3/g; A represents a linear correlation coefficient; p_0 is saturated vapor pressure, MPa. The plots of $\ln V$ versus $\ln(\ln(p_0/p))$ and calculated D_f are shown in Fig. 4 and Table 4. There is a strong linear relationship for all the fitted curves as the

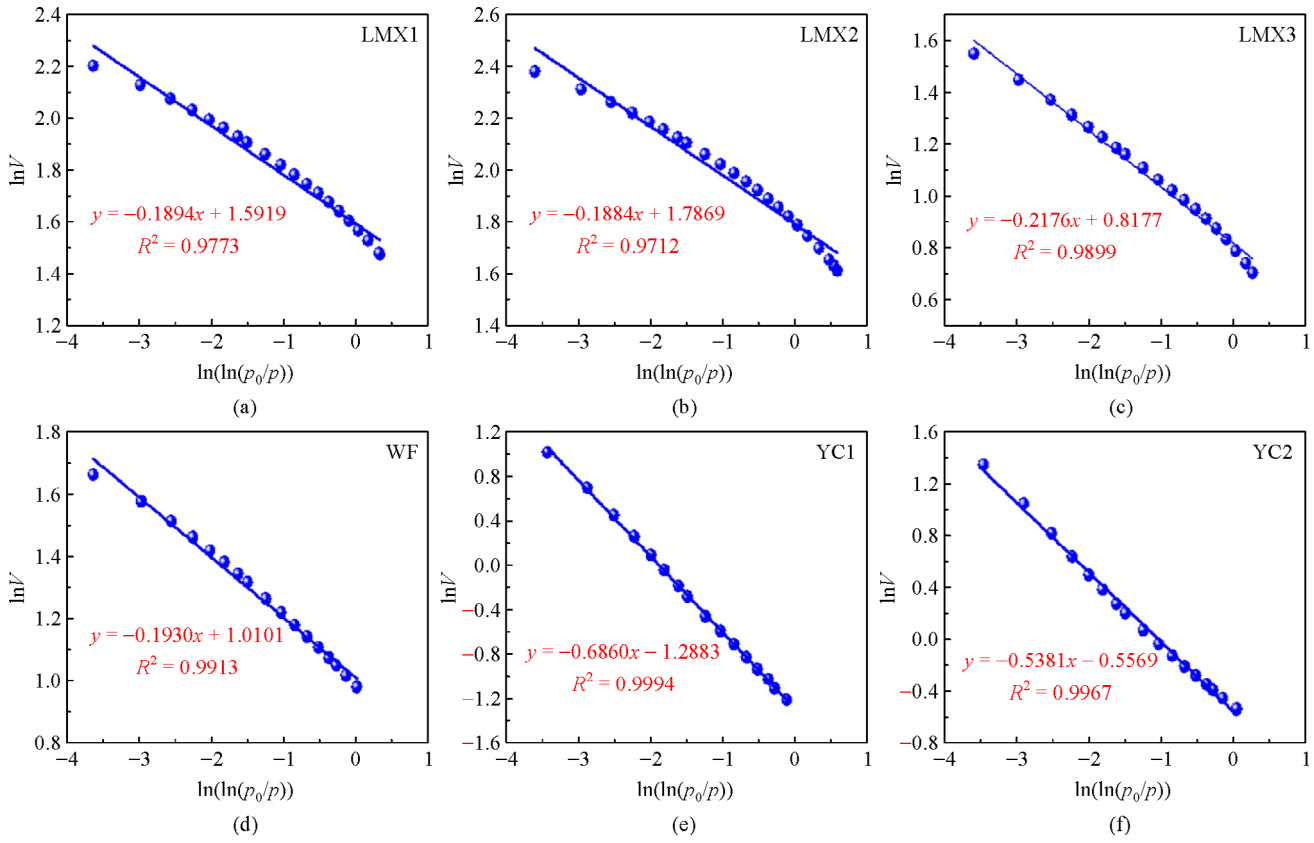

Fig. 4 Fitting plot of $\ln(\ln(p_0/p))$-$\ln V$ based on N_2 adsorption data in shale samples.

Table 4 FFH fractal dimensions D_f, fractal fitting equation and R^2

Sample No.	Fractal fitting equation	D_f	R^2
LMX1	$y = -0.1894x + 1.5919$	2.8106	0.9773
LMX2	$y = -0.1884x + 1.7869$	2.8116	0.9712
LMX3	$y = -0.2176x + 0.8177$	2.7824	0.9899
WF	$y = -0.1930x + 1.0101$	2.8079	0.9913
YC1	$y = -0.6860x - 1.2883$	2.3140	0.9994
YC2	$y = -0.5381x - 0.5569$	2.4619	0.9967

fitting coefficients R^2 were greater than 0.97. Various D_f values reflect the difference in structural complexity of different shale samples. The D_f of the tested shale sample ranges from 2.3140–2.8116, which is between 2 and 3, indicating that the pore structure of shale shows obvious fractal characteristics (Jaroniec, 1995). The D_f of the tested marine shales is larger than that of continental shales, revealing that the pore structure of the marine shale samples is more complex than that of continental shale samples.

3.1.3 Correlations between mineral composition and pore structure of shale

Shale includes minerals and organic matters, both of which have a strong influence on its pore structure. Figure 5 shows the relationship between R_o, TOC and the relevant pore structure parameters of shale. The correlation between R_o and total pore volume, total specific surface area in Fig. 5(a) is not obvious, which may be due to the fact that thermal evolution process has a complex influence on the pore structure. Ma and Guo (2020) observed that when the R_o values ranged in 0.93%–2.76%, there is also no linear correlation between the R_o and the pore volume, which is similar to the tested shale samples in this study. There is a positive correlation between TOC and PV_{mic} (R^2= 0.8426), a weak positive correlation between TOC and PV_{mec} (R^2= 0.4242), and no obvious correlation between TOC and PV_{mac} (R^2= 0.2437) (Fig. 5(b)), which is due to that the organic matter contained abundant micropore in shale.

Generally, organic matter in shale contained much nanopores with the pore size less than 2 nm, so there is a good correlation between TOC and micropore. The positive correlation between SSA_{mic}, SSA_{mes} and TOC in Fig. 5(c) further indicates that organic matter contains abundant micropores and mesopores. It should be noted that TOC also has a good correlation with SSA_{total} (R^2= 0.8073), which further proves that the specific surface area of pores is mainly contributed by micropores and mesopores. Figure 5(d) shows that TOC content was positively correlated with fractal dimension D_f (R^2= 0.7041). The shale with higher TOC content contained more developed organic matter pores, which leads to rougher pore surface and more irregular pore structure, as a higher D_f corresponding to more complex pore structure in shale, thus the D_f increased with the increase of TOC.

Figure 6 shows the effect of clay mineral and brittle mineral contents on the pore structure of shale. The clay mineral content in shale is positively correlated with PV_{total}, PV_{mes} and PV_{mac} in different degrees (R^2 values were 0.8046, 0.8011 and 0.7557, respectively), while the correlation with PV_{mic} was not obvious (R^2= 0.2634) (Fig. 6(c)). And it is also positively correlated with SSA_{total} (R^2= 0.8161), while it is weakly negatively correlated with PD_{ave} (R^2= 0.2790) (Fig. 6(d)). There are two groups of pores in clay minerals: micron-sized pores and nano-sized pores, in which montmorillonite mainly develops micropores, kaolinite mainly develops 20–100 nm intergranular pores, illite and chlorite mainly develop micron-sized macropores (Ji et al., 2012a). The clay minerals in the tested shale samples mainly contain illite and chlorite, and a small amount of montmorillonite (Table 2), therefore, there is an obvious positive relationship between clay mineral content and PV_{mes} and PV_{mac}, while a weak relationship with PV_{mic}. However, clay minerals can fill the macropore space and suppress the development of macropores, thus, there is a negative correlation between the clay minerals content and PD_{ave}.

The content of brittle minerals is negatively correlated with PV_{total} (R^2= 0.7580), PV_{mic} (R^2= 0.8287) and PV_{mes} (R^2= 0.7357). There is also a good negative correlation between SSA_{total} and brittle mineral content (R^2= 0.9730), while the PD_{ave} is positively correlated with the content of brittle minerals (R^2= 0.6691). Wang et al. (2014) argued that per unit mass of organic matter in shale contributed the largest pore volume, followed by clay minerals, then

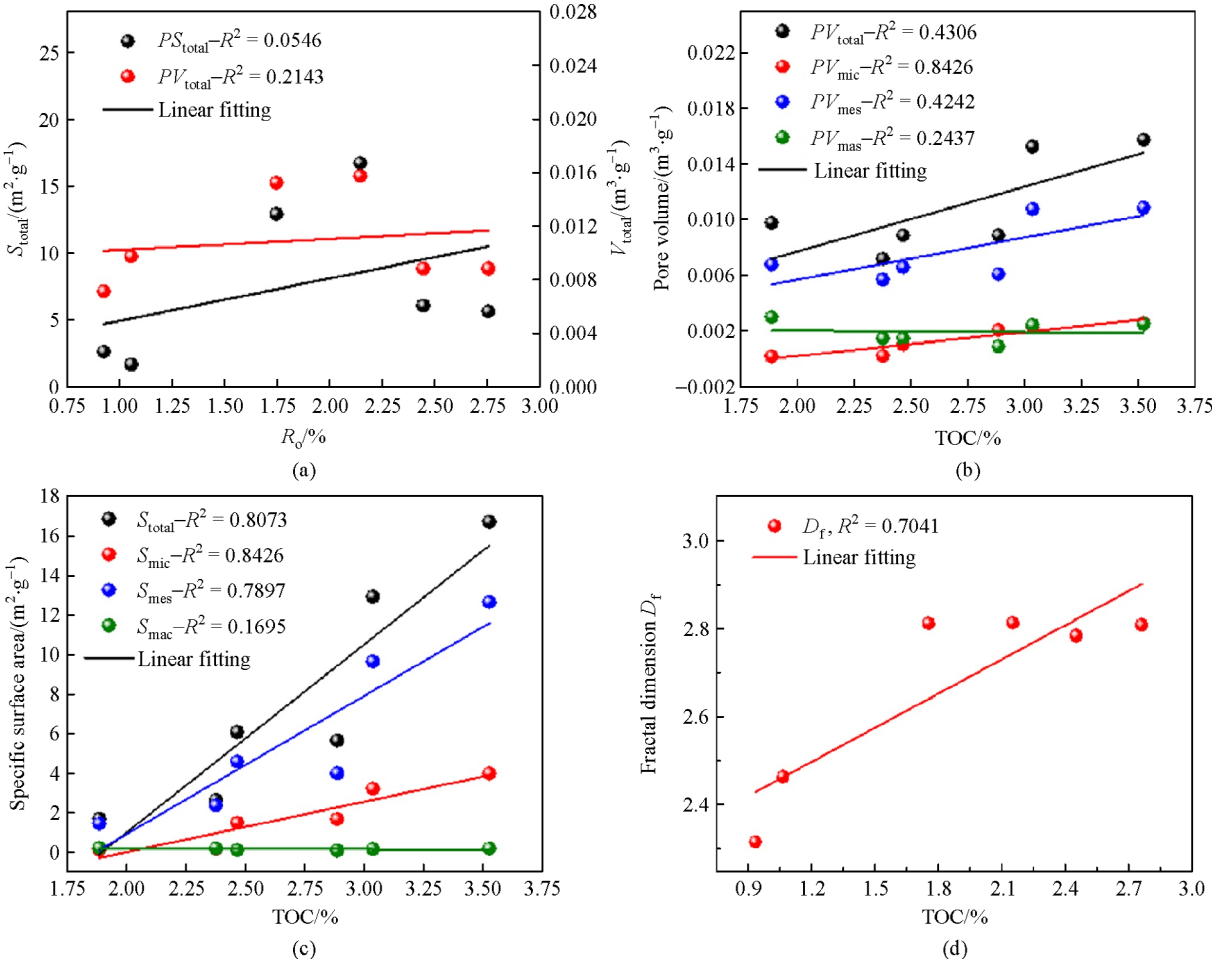

Fig. 5 Relationship between R_o, TOC and pore structure parameters.

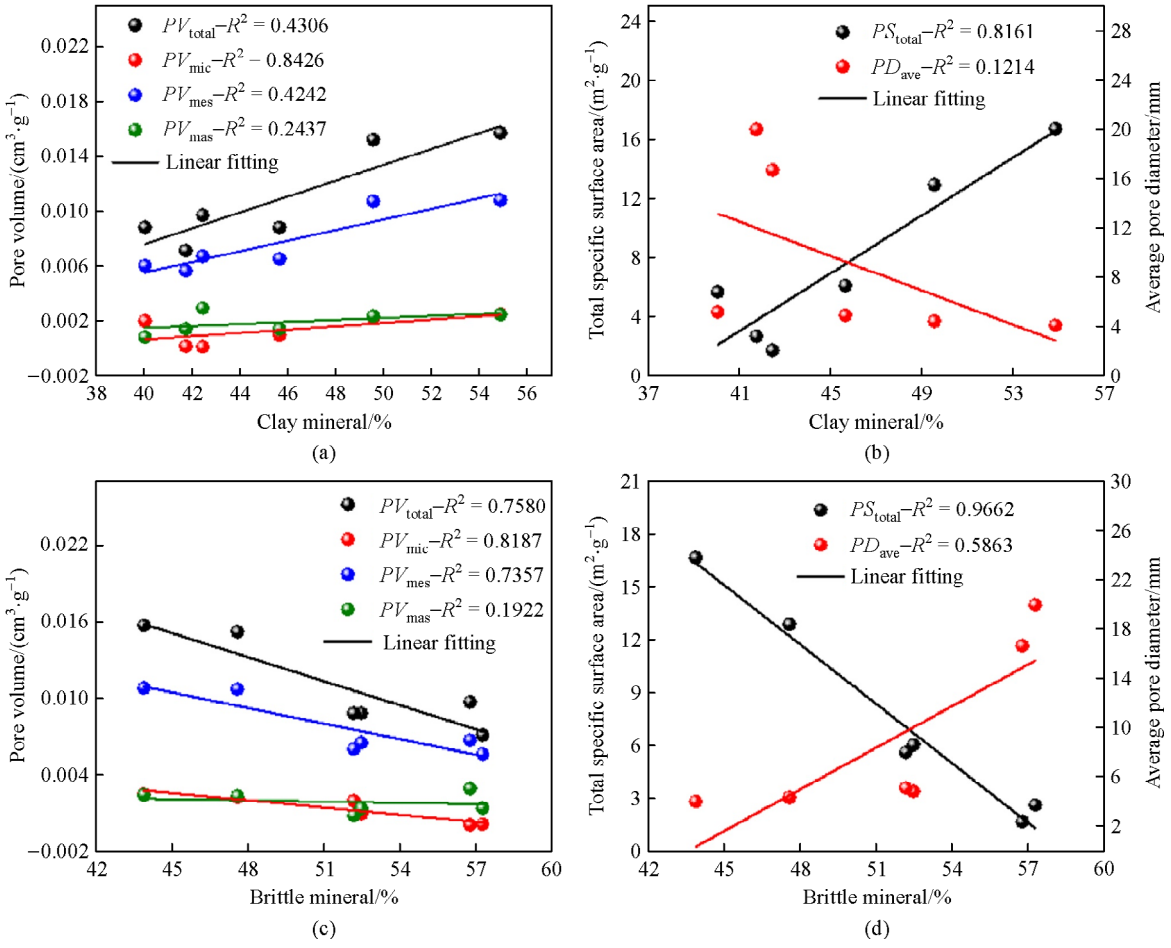

Fig. 6 Relationship between clay minerals, brittle minerals and pore structure parameters.

Table 5 Fitting parameters of Langmuir model for CH_4, CO_2 adsorption isotherms

Sample No.	T/K	Langmuir model fitting parameter					
		CH_4 adsorption			CO_2 adsorption		
		V_L/(mmol·g^{-1})	P_L/MPa	R^2	V_L/(mmol·g^{-1})	P_L/MPa	R^2
LMX1	298.15	0.1282	2.1286	0.9922	0.3253	1.7058	0.9648
	318.15	0.1208	2.9109	0.9968	0.2739	1.8922	0.9777
	338.15	0.1115	3.1434	0.9956	0.2049	2.0284	0.9931
WF	298.15	0.1052	5.1884	0.977	0.2304	3.5506	0.9641
	318.15	0.1030	6.1105	0.9846	0.2075	4.1117	0.9685
	338.15	0.0977	6.9852	0.9877	0.1760	4.3691	0.9780
YC1	298.15	0.0981	4.2005	0.9994	0.2628	1.8178	0.9670
	318.15	0.0940	4.8517	0.9992	0.2213	1.9764	0.9717
	338.15	0.0899	5.5883	0.9988	0.1846	2.1538	0.9848
YC2	298.15	0.0819	5.2670	0.9978	0.2028	1.6650	0.9558
	318.15	0.0802	6.8592	0.9990	0.1850	2.2384	0.9687
	338.15	0.0724	7.5409	0.9988	0.0906	2.2954	0.9901

finally is brittle minerals. Thus, with the increase of brittle minerals, the pore volume of shale was decreased. In addition, diagenesis is also an essential factor affecting pores development in brittle minerals, the majority of the brittle minerals contained in shale is quartz, the authigenic quartz can occupy part of the pore space in shale, resulting in decreases in the *PV* and *SSA* of shale. Nevertheless, there is no apparent correlation between the PV_{mac} and the content of brittle minerals. Overall, the thermal evolution degree, organic matters, clay minerals and brittle minerals content of shale all affect the pores development in shale, however, for different shale samples collected from different geological strata, the main control factor for the pore structure evolution is different, the comprehensive effects of these influencing factors on the pore structure are preferred to be considered.

3.2 Adsorption characteristic of CO_2 and CH_4

3.2.1 Adsorption isotherms of CH_4 and CO_2

The isothermal adsorption curves of CH_4 and CO_2 on shales at different temperatures are shown in Fig 7. At a certain temperature, the CH_4 and CO_2 adsorption capacity were increased with the increase of pressure. The increase rate of CH_4 and CO_2 adsorption volume at low pressure stage is larger than that at high pressure stage, and the increase rate gradually decreases with the increase of pressure. At the higher pressure stage, the CH_4 adsorption isotherm showed a steady upward trend tend to a saturation state, however, the CO_2 adsorption isotherm shown a sustained growth trend in the tested pressure range, which indicated that CO_2 adsorption in shale is far from its saturation adsorption state due to the maximum adsorption pressure is relative low in this study. The adsorption capacities of CH_4 and CO_2 on all the tested shale samples decreased with the increase of temperature. This is because of that the adsorption in shale is an exothermic process, thus at higher temperature is not conducive to gas adsorption, resulting in a lower adsorption of CH_4 and CO_2 at higher temperatures.

The adsorption data of CH_4 and CO_2 on shale were fitted to the commonly used Langmuir model (Langmuir, 1918):

$$V = \frac{V_L P}{P + P_L}, \tag{3}$$

where, V is the adsorption amount at pressure P, mmol/g; V_L is Langmuir volume, which is corresponding to the maximum or total volume of gas that can be adsorbed in shale at infinite pressure, mmol/g; P_L is Langmuir pressure, which is corresponding to the pressure at which one half of the Langmuir volume can be adsorbed, MPa.

The fitting curves of CH_4 and CO_2 adsorption data for the Langmuir model are also shown in Fig. 7 with calculated parameters in Table 5. Langmuir model produce good fits for CH_4 and CO_2 adsorption isotherms in the tested pressure ranges with the fitting coefficient R^2 ranges of 0.9558–0.9970. As shown in Table 5, at the same temperature, the V_L of CO_2 is always greater than that of CH_4 for all the tested shale samples, indicating that the adsorption capacity of CO_2 is greater than that of CH_4. The V_L of CH_4 and CO_2 decreased with the increase of temperature, which is consistent with the variation trend of CH_4 and CO_2 adsorption amount shown in Fig. 7. The P_L of CH_4 is higher than that of CO_2 at the same temperature, P_L reflect the affinity between the adsorbate and the adsorbent, a lower value of P_L imply a greater affinity of the adsorbate towards to the adsorbent (Gensterblum et al., 2013). P_L increased with the increase of temperature, indicating that the increase of temperature will weaken the affinity between gas molecules and shale. Shales from different regions and geological formations show different adsorption capacities of CH_4 and CO_2, thus, when adapting the CO_2-ESGR technology in different shale gas reservoirs, it is essential to study the CH_4 and CO_2 adsorption behavior on a case by case basis.

3.2.2 Effect of mineral compositions on the adsorption capacity of shale

Figure 8 shows the relationship between R_o, TOC and the V_L of CH_4 and CO_2 in shale. As shown in Figs. 8(a) and 8(b), no direct correlation was observed between the adsorption capacity of CH_4 and CO_2 on shale and R_o (R^2 range is 0.2005–0.2989). Klewiah et al. (2020) argued that with the increase of thermal maturity (R_o), organic matter develops micropores as kerogen is thermally converted, and the increase of the amount of micropores improves the adsorption capacity of shale. Nonetheless, the prior analysis in this study illustrated the R_o of selected shale samples has no obvious relationship with the pore structure parameters, then R_o shows no direct correlation with the adsorption capacity of shale. There is a clear linear positive correlation between TOC content and V_L of CH_4 on shale (R^2 is 0.7800–0.9075) (Fig. 8 (c)). Although V_L of CO_2 on shale also increases with the increase of TOC, but the linear relationship is not strong (R^2 is 0.2694–0.6434) (Fig. 8 (d)), which indicated that adsorption of CH_4 in shale shown more significant relationship between TOC content than that of CO_2. Generally, a higher content of TOC corresponding to a more developed organic matter pores with more abundant adsorption sites in shale, thus the V_L of CH_4 and CO_2 were increased with the increase of TOC content, the results are consistent with the findings of Hong et al. (2016). In this study, the linear relationship between TOC and the maximum adsorption capacity of CH_4 is stronger than that of CO_2, indicating that the adsorption capacity of shale to CH_4 is more closely related to TOC. The reason may be due to that organic matter is more inclined to adsorb CH_4 (organic material) than CO_2

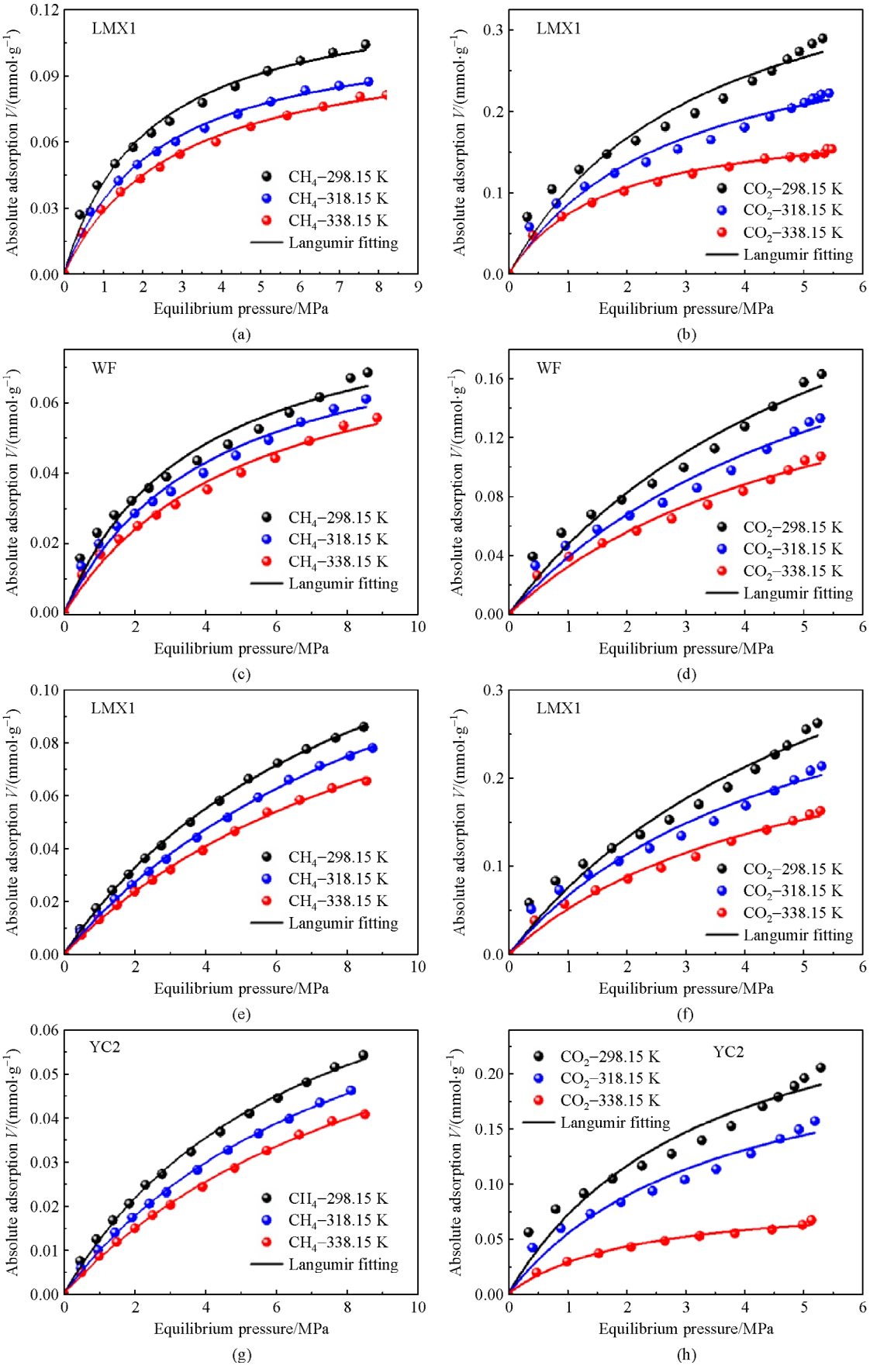

Fig. 7 Langmuir model fitting of CH_4, CO_2 adsorption isotherms at different temperatures.

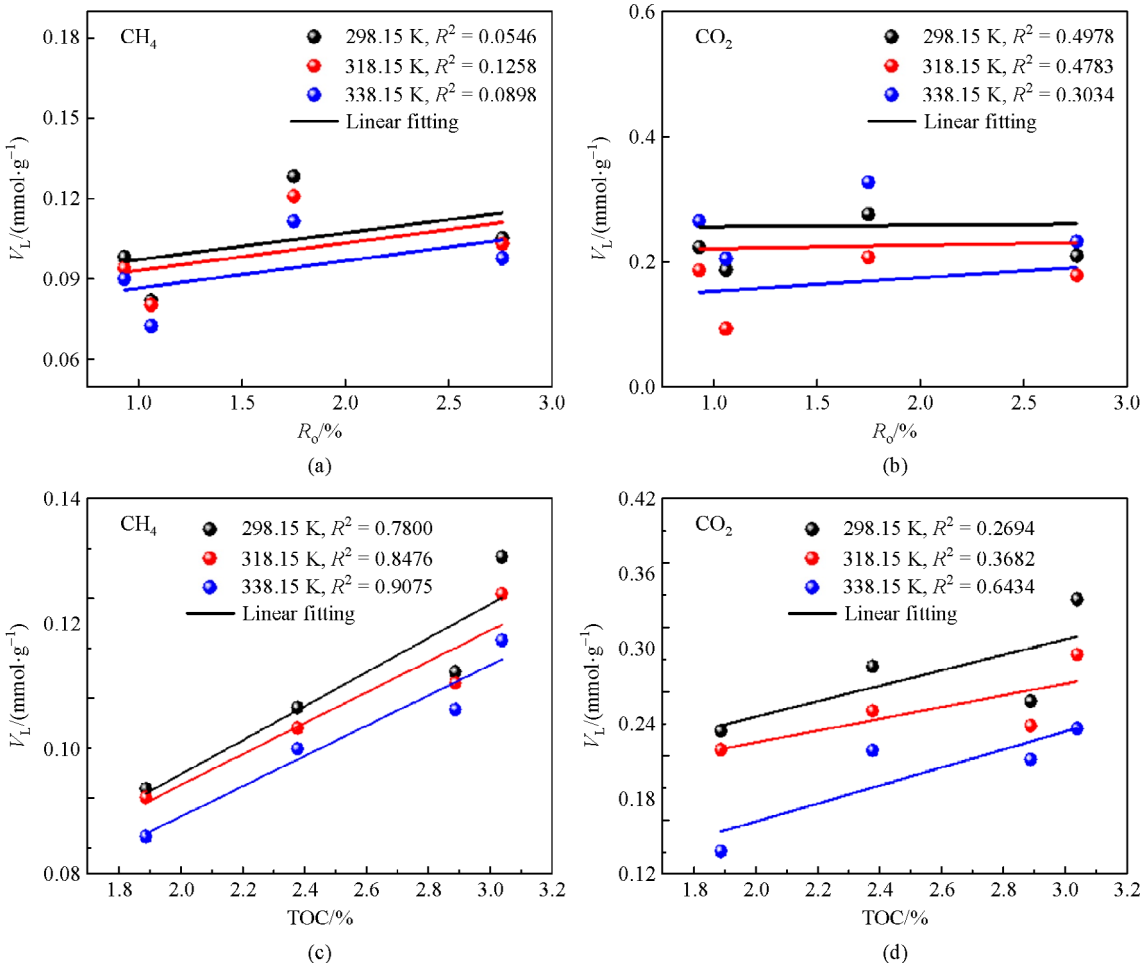

Fig. 8 Relationship between R_o, TOC and maximum adsorption capacity V_L.

(inorganic material), while the inorganic material is more likely to adsorb CO_2 than CH_4 (Ross and Bustin, 2009).

The influence of mineral composition on the CH_4 and CO_2 adsorption capacity in shale are shown in Fig. 9. There is a weak positive correlation between the clay mineral content and the maximum adsorption capacity of CH_4 and CO_2 (Figs. 9(a) and 9(b)). Clay mineral are commonly considered to contain abundant adsorption sites in shale. The influence of clay minerals on the adsorption capacity of shale has two main mechanisms. First, the increase of clay mineral content is conducive to the development of nano-scale pores, thereby improving the gas adsorption capacity of shale. In addition, the strong hydrophilicity of clay minerals makes the adsorption sites more easily occupied by water molecules, which inhibits the adsorption of gas in shale (Passey et al., 2010; Ji et al., 2012a). The samples used in this study are dried before the adsorption measurement, thus the first mechanism plays a dominant role, leading to the gas adsorption capacity increased with the increase of clay minerals content. In addition, many scholars have reported that the effect of clay minerals on the adsorption characteristics of shales is not obvious with high TOC shale, which may be another reason for the weak correlation in this study (Wang et al., 2013; Gasparik et al., 2014; Bi et al., 2016). It should be noted that adsorption capacity of CO_2 shown a more significant correlation with clay minerals than that of CH_4, which may be due to the aforementioned reason that inorganic minerals are more inclined to adsorb CO_2. The V_L of CH_4 and CO_2 in shale is negatively correlated with brittle minerals, which may be due to that the increase of brittle mineral content may lead to the decrease of micropores development, thus caused the decrease of gas adsorption capacity in shale. In addition, the increase of brittle mineral content may cause the decrease of TOC and clay mineral content in shale, thus further decrease the adsorption capacity of shale.

3.2.3 The influence of pore structure on the adsorption capacity of shale

Figures 10, 11(a) and 11(b) show that V_L of CH_4 and CO_2 in shale is positively correlated with both PV_{total} and

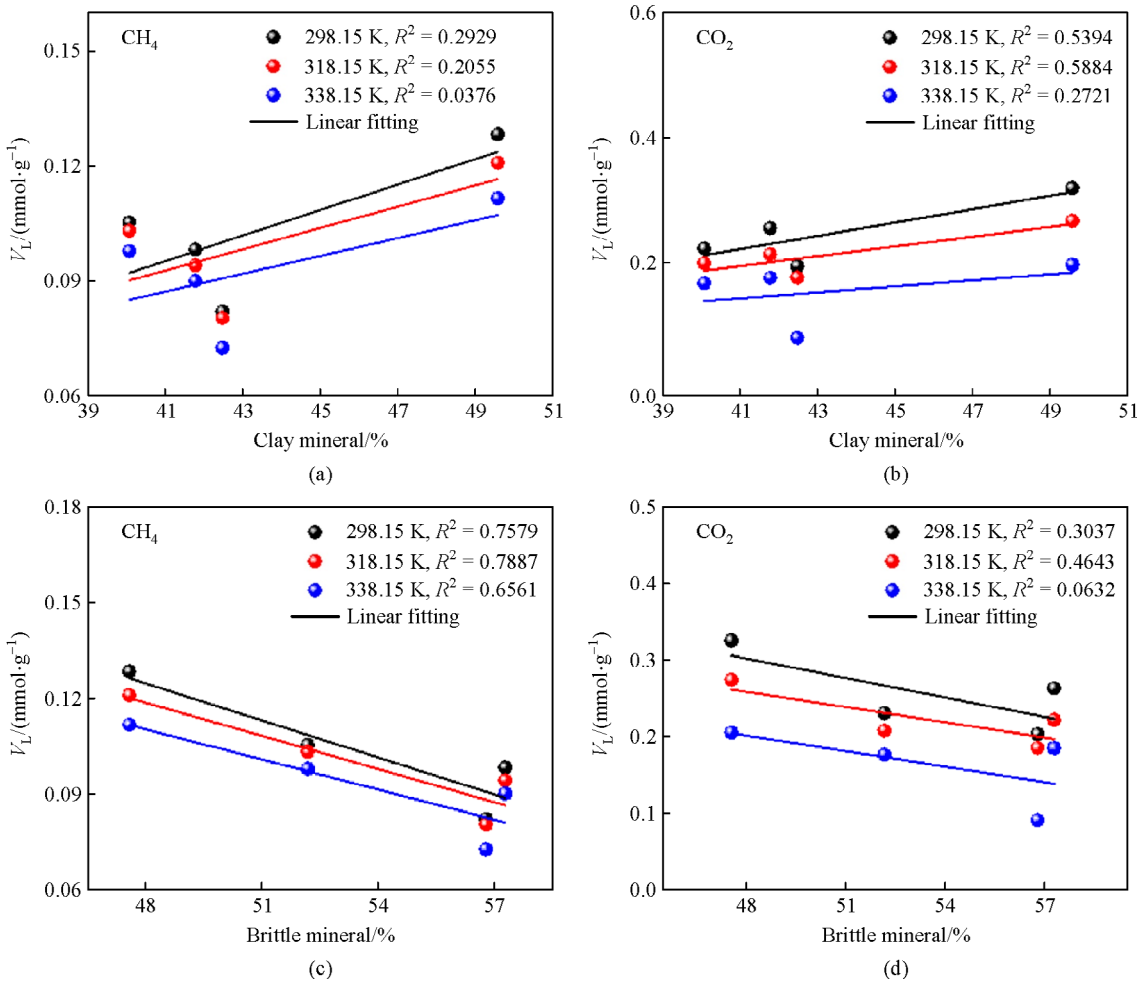

Fig. 9 Relationship between component characteristics and maximum adsorption capacity V_L.

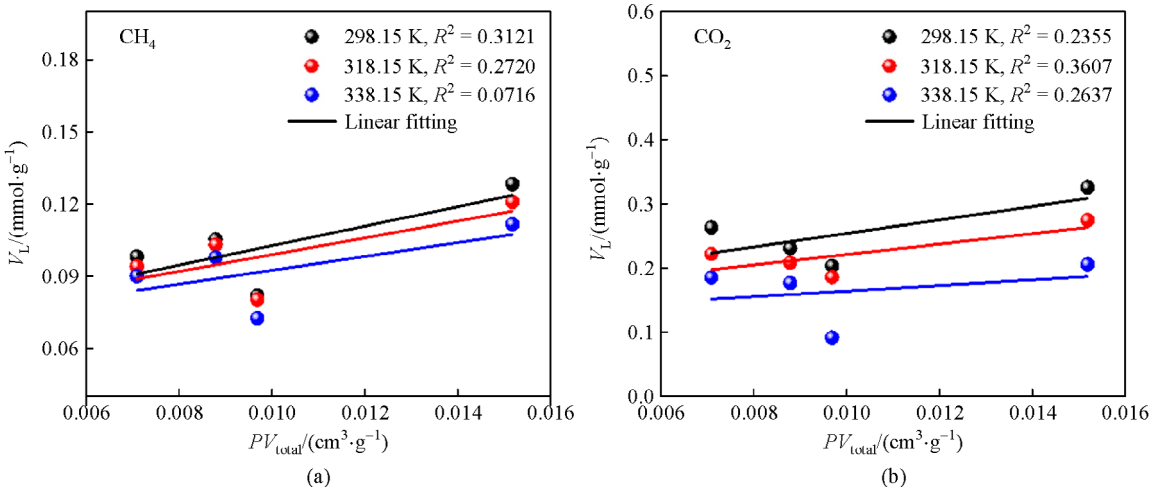

Fig. 10 Relationship between PV_{total} and V_L.

SSA_{total} for a certain temperature, and the correlation between V_L and SSA_{total} is obviously stronger than that between V_L and PV_{total}. Generally, a larger SSA_{total} means more adsorption sites in shale, which is more conducive to gas adsorption in shale. Figure 11 shows that V_L of CH_4 is more significantly related to SSA_{mic} and SSA_{mes} than V_L of

Table 6 α_{CO_2/CH_4} of shale samples at different temperatures

Sample No.	298.15 K	318.15 K	338.15 K
LMX1	3.17	3.49	2.85
WF	3.20	2.99	2.88
YC1	6.19	5.78	5.33
YC2	7.83	7.07	4.11

CO_2. CO_2 and CH_4 adsorption capacity in shale is influenced by comparative effects of organic matter pores and inorganic pores on the adsorption behaviors in shale (Hou et al., 2014). The previous analysis shown that organic matter has stronger affinity for CH_4, while clay minerals have stronger affinity for CO_2. As the micropores and mesopores in shale is mainly contributed by organic matter, thus V_L of CH_4 is more significantly correlated with SSA_{mic} and SSA_{mes} than that of CO_2 (Figs. 11(c) and 11(e)). Figure 11 also shown that the correlation between V_L of CO_2 and SSA_{mes} is the most significant compared with SSA_{mac} and SSA_{mic}, which shown a good consistent with the relationship between clay mineral content and mesopore volume shown in Fig. 6(a). The results also indicated that CO_2 is preferred to be adsorbed on the mesopore contributed by clay mineral and further confirmed that the clay minerals are more likely to adsorb CO_2 than CH_4. It should be noted that the fitting coefficients of the correlation between V_L of CH_4 and CO_2 with SSA_{total}, SSA_{mic}, SSA_{mes} and SSA_{mac} were decreased with the increase of temperature, especially for the cases of CO_2 adsorption at the temperature condition of 338K, the correlation becomes very weak, which indicated that the influence of the temperature on the CO_2 adsorption characteristics is more significant than CH_4, and the adsorption behavior of shale is controlled by the combination effects of shale properties and reservoir conditions.

3.3 Selective adsorption of CO_2 and CH_4 on shale

3.3.1 Selective adsorption coefficient

The selective adsorption coefficient of CO_2 over CH_4 (α_{CO_2/CH_4}) on shale is an important parameter to evaluate the feasibility for CO_2-ESGR technique, which can be obtained as follows (Duan et al., 2016).

$$\alpha_{CO_2/CH_4} = \frac{V_{LCO_2}}{V_{LCH_4}} \cdot \frac{b_{CO_2}}{b_{CH_4}}, \tag{4}$$

where, V_{LCO_2} and V_{LCH_4} are the Langmuir volume of CO_2 and CH_4, mmol/g, respectively, b_{CO_2} and b_{CH_4} are respective fitting constants.

Table 6 shows the α_{CO_2/CH_4} for all the tested samples, it can be observed that α_{CO_2/CH_4} ranges of 2.85–7.83 at various temperatures, which indicated that the adsorption capacity of CO_2 in different types of shale is greater than that of CH_4, thus it is feasible for CO_2 injection to enhance shale gas recovery in these shale formations. At the same temperatures, the α_{CO_2/CH_4} values of continental shale samples are higher than those of marine shale samples, which indicated that the CO_2-ESGR technique is likely more adaptable in continental shale. In addition, it can be seen from Table 6 that α_{CO_2/CH_4} decreased with increasing temperature for most cases, which may due to that the interaction force of CO_2-shale decreased more significant than that of CH_4-shale with the increase of temperature. Therefore, a lower temperature is more favorable for the application of CO_2-ESGR technique.

3.3.2 Effect of mineral compositions on α_{CO_2/CH_4} in shale

Figure 12 shows the relationship of R_o, TOC, clay mineral content, brittle mineral content and α_{CO_2/CH_4} in shale. Figures 12(a) and 12(b) show that α_{CO_2/CH_4} is negatively correlated with R_o and TOC at the various temperatures. Although the relationship between R_o and the adsorption of CO_2 and CH_4 is not obvious, there is a weak negative correlation between R_o and α_{CO_2/CH_4} (R^2 is 0.4189–0.5222). Especially at the temperatures of 298.15K and 318.15K, α_{CO_2/CH_4} and TOC shown more significant correlations (R^2 is 0.9662 and 0.9066, respectively), which is due to organic matter is more likely to adsorb CH_4, and this result is also consistent with the stronger correlation between TOC and CH_4 maximum adsorption capacity obtained above. The correlation between α_{CO_2/CH_4} and TOC decreases significantly at 338.15K (R^2= 0.1751), indicating that the effect of temperature on the relationship between α_{CO_2/CH_4} and TOC cannot be ignored. Figure. 12(c) shown that shale with a higher brittle mineral content corresponding to a higher α_{CO_2/CH_4}, which may be due to the more significant negative correlation between V_L of CH_4 and brittle minerals than that of CO_2. However, in Fig. 12(d), there is no obvious correlation between α_{CO_2/CH_4} and clay mineral content in shale. The component of clay minerals in shale is complex, the α_{CO_2/CH_4} of different pure component is varied widely. The adsorption capacity of illite and kaolinite for CO_2 is about 1.5 times and 4.0 times of that for CH_4, respectively (Heller and Zoback, 2014). Marine shale has higher content of illite and lower content of kaolinite than continental shale, which contributes to the higher α_{CO_2/CH_4} in continental shale (Table 6).

3.3.3 Effect of pore structure on α_{CO_2/CH_4} of shale

The correlations between α_{CO_2/CH_4} and PV_{total}, PV_{mic}, SSA_{total} and SSA_{mic} are shown in Figs. 13(a)–13(d), and the negative correlations were observed between α_{CO_2/CH_4} and these parameters. The negative correlation between PV_{total}, SSA_{total} and α_{CO_2/CH_4} is less pronounced ($R^2 \leqslant 0.4568$),

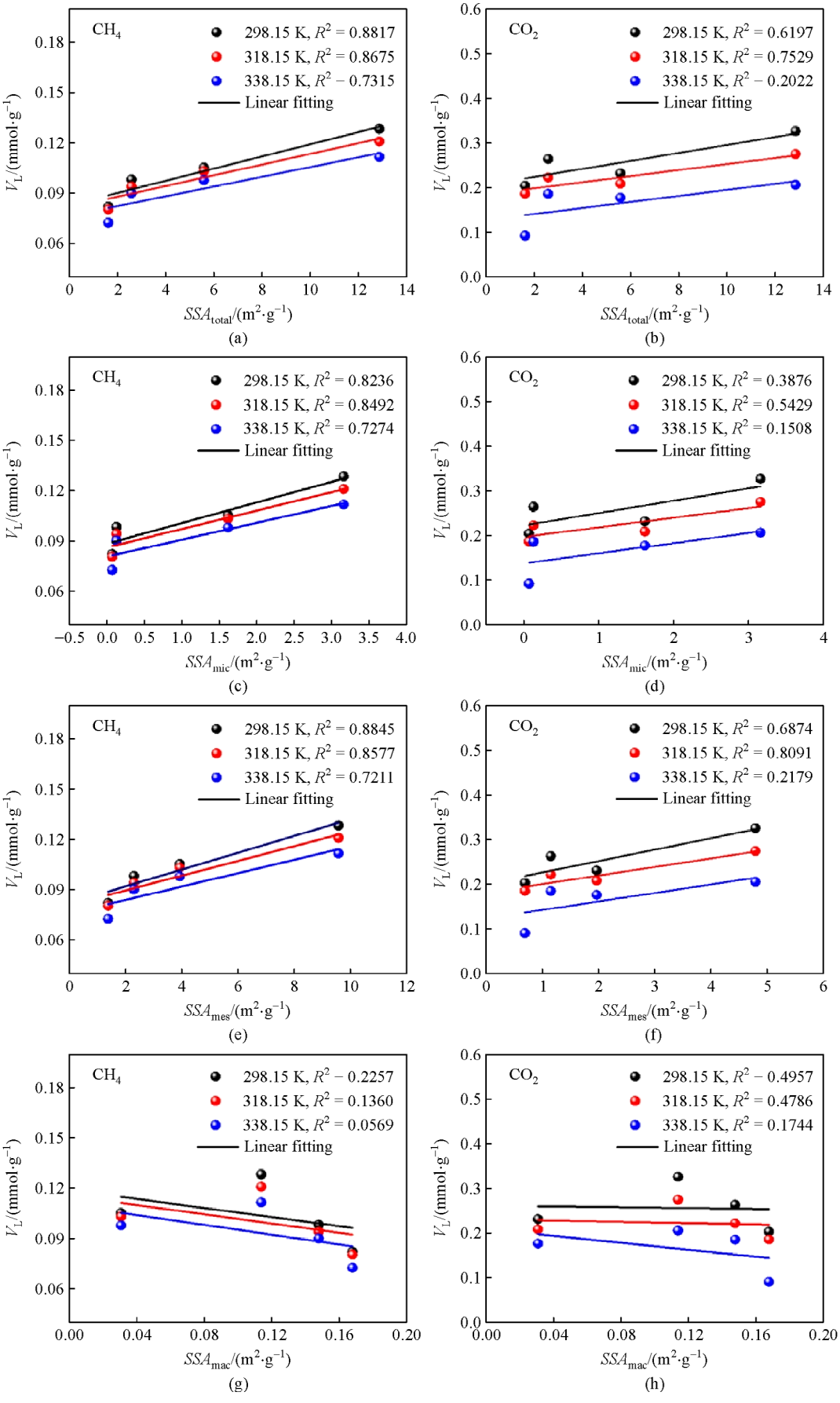

Fig. 11 Relationship between pore specific surface area and V_L.

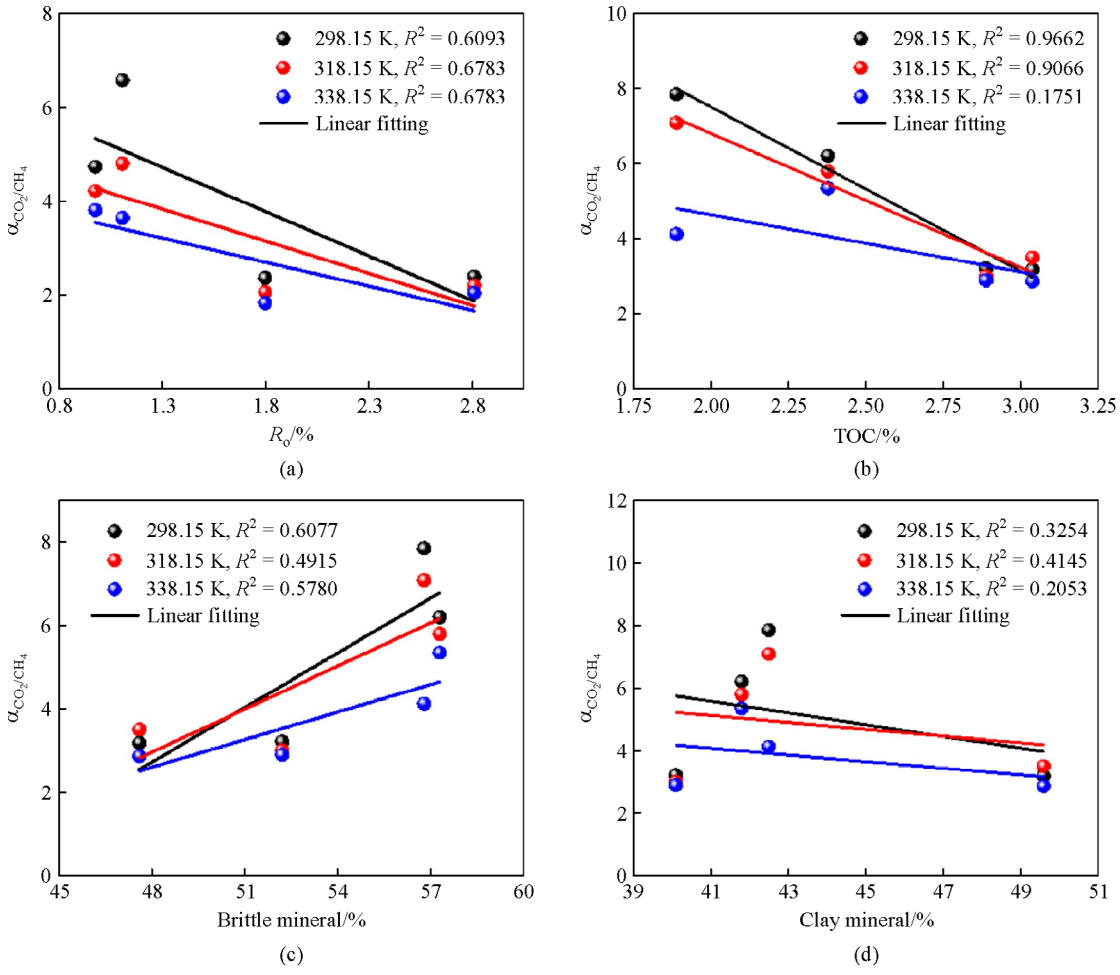

Fig. 12 Relationship between mineral compositions and α_{CO_2/CH_4}.

while the relationship between PV_{mic}, SSA_{mic} and α_{CO_2/CH_4} is more obvious (R^2 = 0.7054–0.8758 and 0.4989–0.6363 respectively). This is because the micropores associated with the organic components in the shale are favorable for the adsorption of CH_4, resulting in the decrease of α_{CO_2/CH_4} with the increase of PV_{mic} and SSA_{mic}. The TOC value and micropore volume of marine shale are larger than those of continental shale, which leads to the α_{CO_2/CH_4} of marine shale is smaller than that of continental shale at same temperature. Figure 13(e) shows α_{CO_2/CH_4} is negative correlated with fractal dimension D_f of pore structure, as D_f can reflect the complexity and heterogeneity of pore structure, and is closely related to the organic matter and mineral content in shale, thus it can be used as a parameter to qualitatively characterize the α_{CO_2/CH_4} of shale.

4 Conclusions

In this study, the adsorption behaviors of CH_4 and CO_2 were invested by using the marine shales of Wufeng-Longmaxi formation and the continental shales of Yanchang formation. The main conclusions are as follows.

1) Shale with higher TOC, higher content of clay minerals and lower content of brittle mineral has a larger micropores and mesopores volume and specific surface area, and shale with higher TOC content has larger fractal dimension D_f of pore structure.

2) The contents of TOC and clay minerals are positively correlated with the adsorption capacity of CH_4 and CO_2 in shale, and the correlation of the contents of clay minerals is weak. This is because the shale with higher TOC and clay mineral content corresponds to higher specific surface area, which can provide more adsorption sites for CH_4 and CO_2 in shale. The relationship between TOC and the maximum adsorption capacity of CH_4 is stronger than that of CO_2, while CO_2 adsorption capacity shown a more significant correlation with clay minerals than CH_4, which may be due to that organic matter is more inclined to adsorb CH_4 than CO_2, while the inorganic material such as clay mineral is more likely to adsorb CO_2 than CH_4.

3) All the α_{CO_2/CH_4} of shale were larger than 1.00, which

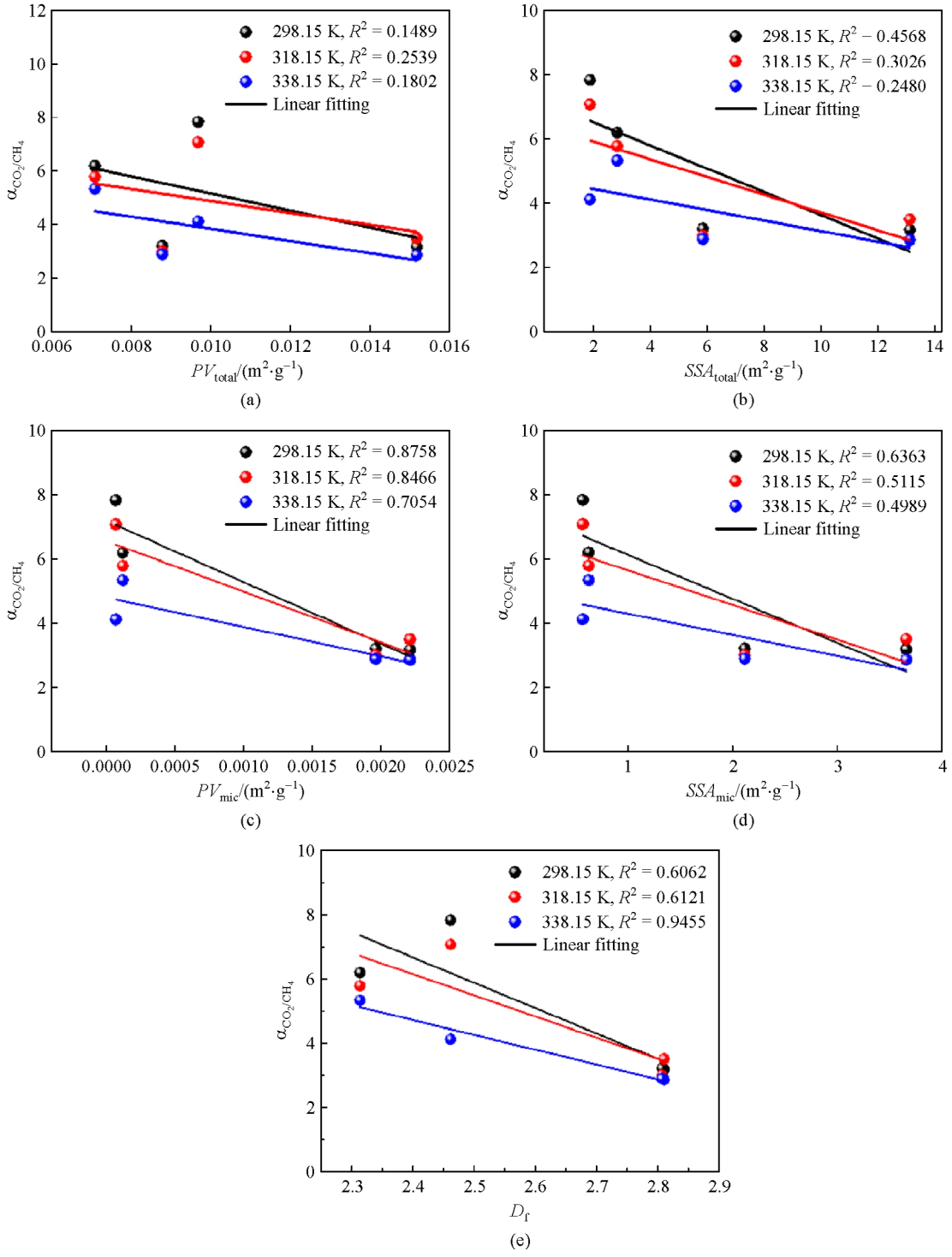

Fig. 13 Relationship between pore structure parameters and α_{CO_2/CH_4}.

indicated the feasibility of application of CO_2-ESGR technology in these shale gas reservoirs. The shale with higher TOC content and brittle mineral content shows higher α_{CO_2/CH_4} values, while there is no obvious correlation between α_{CO_2/CH_4} and clay mineral content in shale. The α_{CO_2/CH_4} of shale were decreased with increasing temperature for most cases, which indicated that a lower temperature is more favorable for the application of CO_2-ESGR technique.

Acknowledgements This study was financially supported by the National Natural Science Foundation of China (Grant Nos. 51774060, U19B2009), the

Program for Changjiang Scholars and Innovative Research Team in University (IRT_17R112), the Basic Research and Frontier Exploration Projects in Chongqing (cstc2019jcyj-msxmX0053, cstc2019yszx-jcyjX0007), Shaanxi Innovation Capability Support Plan (2019KJXX-023).

References

Bi H, Jiang Z, Li J, Li P, Chen L, Pan Q, Wu Y (2016). The Ono–Kondo model and an experimental study on supercritical adsorption of shale gas: a case study on Longmaxi shale in southeastern Chongqing, China. J Nat Gas Sci Eng, 35: 114–121

Brunauer S, Emmett P H, Teller E (1938). Adsorption of gases in multimolecular layers. J Am Chem Soc, 60(2): 309–319

Cai Y, Liu D, Pan Z, Yao Y, Li J, Qiu Y (2013). Pore structure and its impact on CH_4 adsorption capacity and flow capability of bituminous and subbituminous coals from Northeast China. Fuel, 103: 258–268

Charoensuppanimit P, Mohammad S A, Gasem K A M (2016). Measurements and modeling of gas adsorption on shales. Energy Fuels, 30: 2309–2319

Cui J, Zhu R, Mao Z, Li S (2019). Accumulation of unconventional petroleum resources and their coexistence characteristics in Chang7 shale formations of Ordos Basin in central China. Front Earth Sci, 13 (3): 575–587

Dayal A M (2017). Chapter 10-role of nonconventional shale gas energy in the next century. Shale Gas Explor Environ Econ Imp, 157–164

Du X, Gu M, Hou Z, Liu Z, Wu T (2019). Experimental study on the kinetics of adsorption of CO_2 and CH_4 in gas-bearing shale reservoirs. Energy Fuels, 33(12): 12587–12600

Duan S, Gu M, Du X, Xian X (2016). Adsorption equilibrium of CO_2 and CH_4 and their mixture on Sichuan Basin shale. Energy Fuels, 30 (3): 2248–2256

Feng G, Zhu Y, Wang G G X, Chen S, Wang Y, Ju W (2019). Supercritical methane adsorption on overmature shale: effect of pore structure and fractal characteristics. Energy Fuels, 33(9): 8323–8337

Gasparik M, Bertier P, Gensterblum Y, Ghanizadeh A, Krooss B M, Littke R (2014). Geological controls on the methane storage capacity in organic-rich shales. Int J Coal Geol, 123: 34–51

Gensterblum Y, Merkel A, Busch A, Krooss B M (2013). High-pressure CH_4 and CO_2 sorption isotherms as a function of coal maturity and the influence of moisture. Int J Coal Geol, 118: 45–57

Gu M, Xian X, Duan S, Du X (2017). Influences of the composition and pore structure of a shale on its selective adsorption of CO_2 over CH_4. J Nat Gas Sci Eng, 46: 296–306

Heller R, Zoback M (2014). Adsorption of methane and carbon dioxide on gas shale and pure mineral samples. J Unconv Oil Gas Resour, 8: 14–24

Hong L, Jain J, Romanov V, Lopano C, Disenhof C, Goodman A, Hedges S, Soeder D, Sanguinito S, Dilmore R (2016). An investigation of factors affecting the interaction of CO_2 and CH_4 on shale in Appalachian Basin. J Unconv Oil Gas Resour, 14: 99–112

Hou H, Shao L, Li Y, Li Z, Zhang W, Wen H (2018). The pore structure and fractal characteristics of shales with low thermal maturity from the Yuqia Coalfield, northern Qaidam Basin, northwestern China. Front Earth Sci, 12(1): 148–159

Hou Y, He S, Yi J, Zhang B, Chen X, Wang Y, Zhang J, Cheng C (2014). Effect of pore structure on methane sorption potential of shales. Pet Explor Dev, 41: 272–281

Iddphonce R, Wang J, Zhao L (2020). Review of CO_2 injection techniques for enhanced shale gas recovery: prospect and challenges. J Nat Gas Sci Eng, 77: 103240

Jaroniec M (1995). Evaluation of the fractal dimension from a single adsorption isotherm. Langmuir, 11: 2316–2317

Ji L, Qiu J, Xia Y, Zhang T (2012a). Micro-pore characteristics and methane adsorption properties of common clay minerals by electron microscopy canning. Acta Petrol Sin, 33(2): 249–256 (in Chinese)

Jiao F (2019). Theoretical insights, core technologies and practices concerning “volume development” of shale gas in China. Nat Gas Ind B, 6(6): 525–538

Keshavarz A, Sakurovs R, Grigore M, Sayyafzadeh M (2017). Effect of maceral composition and coal rank on gas diffusion in Australian coals. Int J Coal Geol, 173: 65–75

Klewiah I, Berawala D S, Alexander Walker H C, Andersen P Ø, Nadeau P H (2020). Review of experimental sorption studies of CO_2 and CH_4 in shales. J Nat Gas Sci Eng, 73: 103045

Kuang L, Dong D, He W, Wen S, Sun S, Li S, Qiu Z, Liao X, Li Y, Wu J, Zhang L, Shi Z, Guo W, Zhang S (2020). Geological characteristics and development potential of transitional shale gas in the east margin of the Ordos Basin, NW China. Pet Explor Dev, 47(3): 471–482

Langmuir I (1918). The adsorption of gases on plane surfaces of glass, mica and platinum. J Am Chem Soc, 40(9): 1361–1403

Li A, Ding W, He J, Dai P, Yin S, Xie F (2016). Investigation of pore structure and fractal characteristics of organic-rich shale reservoirs: a case study of lower Cambrian Qiongzhusi formation in Malong block of eastern Yunnan Province, South China. Mar Pet Geol, 70: 46–57

Li X, Elsworth D (2015). Geomechanics of CO_2 enhanced shale gas recovery. J Nat Gas Sci Eng, 26: 1607–1619

Li Z, Shen X, Qi Z, Hu R (2018). Study on the pore structure and fractal characteristics of marine and continental shale based on mercury porosimetry, N_2 adsorption and NMR methods. J Nat Gas Sci Eng, 53: 12–21

Li Y, Wang Z, Pan Z, Niu X, Yu Y, Meng S (2019). Pore structure and its fractal dimensions of transitional shale: a cross section from east margin of the Ordos Basin, China. Fuel, 241: 417–431

Li Y, Yang J, Pan Z, Tong W (2020b). Nanoscale pore structure and mechanical property analysis of coal: an insight combining AFM and SEM images. Fuel, 260: 116352

Liu J, Hui Xie X, Wang Q, Chen S, Hu Z (2020). Influence of pore structure on shale gas recovery with CO_2 sequestration: insight into molecular mechanisms. Energy Fuels, 34: 1240–1250

Liu J, Xie L, Elsworth D, Gan Q (2019). CO_2/CH_4 competitive adsorption in shale: implications for enhancement in gas production and reduction in carbon emissions. Environ Sci Technol, 53(15): 9328–9336 PMID:31318200

Liu Y, Hou J (2020). Selective adsorption of CO_2/CH_4 mixture on clay-rich shale using molecular simulations. J CO_2 Util, 39: 101143

Lu X, Li F, Watson A T (1995). Adsorption studies of natural gas storage in Devonian shales. SPE Form Eval, 10(2): 109–113

Ma X, Guo S (2020). Study on pore evolution and diagenesis division of a Permian Longtan transitional shale in Southwest Guizhou, China. Energy Sci Eng, 00: 1–22

Pang F, Zhang Z, Zhang J, Chen K, Shi D, Bao S, Li S, Guo T (2020).

Progress and prospect on exploration and development of shale gas in the Yangtze River economic belt. J China Univ Geosci, 45(6): 2152–2159

Passey Q R, Bohacs K M, Esch W L, Klimentidis R (2010). From oil-prone source rock to gas-producing shale reservoir—geologic and petrophysical characterization of unconventional shale-gas reservoirs. Soc Petrol Engi, 13150: 1–29

Pei P, Ling K, He J, Liu Z (2016). Shale gas reservoir treatment by a CO_2-based technology. J Nat Gas Sci Eng, 26: 1595–1606

Pomonis P J, Tsaousi E T (2009). Frenkel-Halsey-Hill equation, dimensionality of adsorption, and pore anisotropy. Langmuir, 25 (17): 9986–9994

Qi R, Ning Z, Wang Q, Zeng Y, Huang L, Zhang S, Du H (2018). Sorption of methane, carbon dioxide, and their mixtures on shales from Sichuan Basin, China. Energ Fuels, 32: 2926–2940

Qin C, Jiang Y, Luo Y, Zhou J, Liu H, Song X, Li D, Zhou F, Xie Y (2020). Effect of supercritical CO_2 saturation pressures and temperatures on the methane adsorption behaviours of Longmaxi shale. Energy, 206: 118150

Ross D J K, Bustin R M (2009). The importance of shale composition and pore structure upon gas storage potential of shale gas reservoirs. Mar Pet Geol, 26: 916–927

Shan C, Zhang T, Wei Y, Zhang Z (2017). Shale gas reservoir characteristics of Ordovician-Silurian formations in the central Yangtze area, China. Front Earth Sci, 11(1): 184–201

Shcherba V A, Butolin A P, Zieliński A (2019). Current state and prospects of shale gas production. In: IOP Conference Series: Earth Env Sci, 272

Sing K S W (1982). Reporting physisorption data for gas/solid systems with special reference to the determination of surface area and porosity (Provisional). Pure Appl Chem, 54(11): 2201–2218

Slatt R M, O'Brien N R (2011). Pore types in the Barnett and Woodford gas shales: contribution to understanding gas storage and migration pathways in fine-grained rocks geohorizon. AAPG Bull, 95(12): 2017–2030

Thommes M, Kaneko K, Neimark A V, Olivier J P, Rodriguez-Reinoso F, Rouquerol J, Sing K S (2015). Physisorption of gases, with special reference to the evaluation of surface area and pore size distribution (IUPAC Technical Report). Pure Appl Chem, 87(9 – 10): 1051–1069

Wang J, Guo S (2020). Comparison of geochemical characteristics of marine facies, marine-continental transitional facies and continental facies shale in typical areas of China and their control over organic-rich shale. Energ Source Part A: 1–13

Wang M, Guo Z, Jiao C, Lu S, Li J, Xue H, Li J, Li J, Chen G (2019a). Exploration progress and geochemical features of lacustrine shale oils in China. J Petrol Sci Eng, 178: 975–986

Wang S, Song Z, Cao T, Song X (2013). The methane sorption capacity of Paleozoic shales from the Sichuan Basin, China. Mar Pet Geol, 44: 112–119

Wang Y, Dong D, Yang H, He L, Wang S, Huang J, Pu B, Wang S (2014). Quantitative characterization of reservoir space in the Lower Silurian Longmaxi Shale, southern Sichuan, China. Sci China Earth Sci, 57(2): 312–322

Wang Y, Zhu Y, Liu S, Zhang R (2016). Methane adsorption measurements and modeling for organic-rich marine shale samples. Fuel, 172: 301–309

Yang C, Zhang J, Tang X, Ding J, Zhao Q, Dang W, Chen H, Su Y, Li B, Lu D (2017). Comparative study on micro-pore structure of marine, terrestrial, and transitional shales in key areas, China. Int J Coal Geol, 171: 76–92

Zeng S, Gu J, Yang S, Zhou H, Qian Y (2019). Comparison of techno-economic performance and environmental impacts between shale gas and coal-based synthetic natural gas (SNG) in China. J Clean Prod, 215: 544–556

Zhang J, Tang Y, He D, Sun P, Zou X (2020). Full-scale nanopore system and fractal characteristics of clay-rich lacustrine shale combining FE-SEM, nano-CT, gas adsorption and mercury intrusion porosimetry. Appl Clay Sci, 196: 105748

Zhang Q, Liu R H, Pang Z L, Lin W, Bai W H, Wang H Y (2016). Characterization of microscopic pore structures in Lower Silurian black shale (S11), southeastern Chongqing, China. Mar Pet Geol, 71: 250–259

Zhou J, Hu N, Xian X, Zhou L, Tang J, Kang Y, Wang H (2019a). Supercritical CO_2 fracking for enhanced shale gas recovery and CO_2 sequestration: results, status and future challenges. Adv Geo-Energ Res, 3(2): 207–224

Zhou J, Jin Z, Luo K H (2019b). Effects of moisture contents on shale gas recovery and CO_2 sequestration. Langmuir, 35(26): 8716–8725

Zhou J, Liu M, Xian X, Jiang Y, Liu Q, Wang X (2019c). Measurements and modelling of CH_4 and CO_2 adsorption behaviors on shales: implication for CO_2 enhanced shale gas recovery. Fuel, 251: 293–306

Zhou J, Liu Q, Tan J, Jiang Y, Xian X, Yin H, Ju Y (2017). Pore structure and adsorption characteristics of marine and continental shale in China. J Nanosci Nanotechnol, 17(9): 6356–6366

Zhou J, Xie S, Jiang Y, Xian X, Liu Q, Lu Z, Lyu Q (2018). Influence of supercritical CO_2 exposure on CH_4 and CO_2 adsorption behaviors of shale: implications for CO_2 sequestration. Energ Fuels, 32: 6073–6089

Zhou J, Tian S, Zhou L, Xian X, Yang K, Jiang Y, Zhang C, Guo Y (2020). Experimental investigation on the influence of sub- and super-critical CO_2 saturation time on the permeability of fractured shale. Energ, 191: 116574

Zou C, Dong D, Wang S, Li J, Li X, Wang Y, Li D, Cheng K (2010). Geological characteristics, formation mechanism and resource potential of shale gas in China. Pet Explor Dev, 37(6): 641–653